Network: Comput. Neural Syst. **8** (1997) 107–126. Printed in the UK PII: S0954-898X(97)80750-6

A neuronal model of stroboscopic alternative motion

A Bartsch† and J L van Hemmen‡

Physik-Department T35, Technische Universität München, D-85747 Garching, Germany

Received 8 January 1997

Abstract. A visual stimulus consisting of two alternating images, presented with an intermediate blank phase between each image, each showing a pair of illuminated spots located at opposite corners of an imaginary rectangle, will evoke the percept of either a horizontal or a vertical apparent motion, called 'stroboscopic alternative motion' (SAM). Psychological analyses have revealed that subjects can perceive only one of the two directions of motion at a time, favouring the direction along the shorter edge of the rectangle, but report spontaneous changes between the alternatives. If the stimulus configuration is gradually modified during stimulus presentation so that the preferred direction of motion changes from horizontal to vertical, or vice versa, subjects normally experience a corresponding change of their percept. This change, however, usually occurs with hysteresis, i.e. when the stimulus is significantly beyond its symmetric configuration. In this paper a microscopic neural model is presented which reproduces the main psychological findings. Its essential ingredients are simple motion detectors based on spatiotemporal receptive fields and an inhibition of detectors tuned to orthogonal directions of motion. The response of our network to the SAM stimulus is a high activity of either the detectors tuned to horizontal motion or those tuned to vertical motion, signalling a unique percept. In agreement with experimental studies, the preferred direction of motion is along the shorter edge of non-symmetrical stimuli and perceptual changes occur with hysteresis for a gradually changing stimulus configuration. We finish our argument by developing a mathematically tractable two-neuron model that captures the essentials of the above setup.

1. Introduction

An increasing number of publications are concerned with the psychological and physiological processes relevant to the perception of ambiguous figures. An ambiguous, or ambivalent or reversible, figure is a visual stimulus configuration that is consistent with two or more different perceptual interpretations at the same time. Probably the most prominent, and oldest, example is the Necker cube (Necker 1832, see figure 1, left panel), which appears to the observer as the perspective of a cube as seen from above or below, respectively. Apart from ambivalent figures based on a perspective inversion there are different ones which are reversible due to figure-ground or semantic ambiguities (cf Jastrow 1900, Wallach and Austin 1954, Botwinick 1961, Bugelski and Alampay 1961, Rubin 1921, Attneave 1971, Rock *et al* 1994). Examples can be found in figure 1.

As to the perception of reversible figures, experimental analyses have revealed three different phenomena. These are the *uniqueness* of stimulus interpretation, i.e. at a given time a subject can perceive only one of the possible meanings of the stimulus, *spontaneous changes* of the interpretation (Marbe 1893, Eichler 1930, Köhler 1940, Köhler and Wallach

† E-mail: Armin.Bartsch@physik.tu-muenchen.de
‡ E-mail: Leo.van.Hemmen@physik.tu-muenchen.de

0954-898X/97/020107+20$19.50

Figure 1. Examples of reversible figures. Left panel: perspective of a cube as seen from above or below (Necker 1832). Centre panel: young or old lady (Hill 1915, 'My wife and my mother in law'). Right panel: vase or two faces (after Rubin 1921).

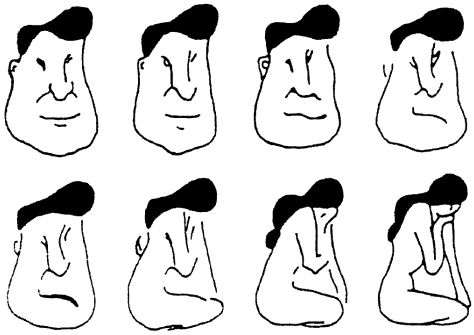

Figure 2. Hysteresis. The place of the perceptual change is dependent on the direction in which the sequence of images is viewed. Taken from Ditzinger and Haken (1989), p 282, figure 5 (copyright: Springer-Verlag).

1944, Orbach *et al* 1963, Stadler and Erke 1968, Pöppel 1982) and *hysteresis* (Wertheimer 1923, Epstein and Rock 1960, Attneave 1971, Kawamoto and Anderson 1985). Hysteresis is found if, instead of a single reversible figure, a series of images is presented ranging from an unambiguous stimulus over different ambivalent versions to another unambiguous figure. Usually under this condition subjects experience a change of their percept only shortly before the second unambiguous stimulus is reached. The same is true if the sequence of images is reversed. Figure 2 shows an example.

Experiments concerning the 'stroboscopic alternative motion' (henceforth SAM) have demonstrated that ambiguity is not restricted to static visual stimuli (von Schiller 1933, Hoeth 1968, Ramachandran and Anstis 1983, Ramachandran and Anstis 1985, Kruse *et al* 1986, Ramachandran 1992, Hock *et al* 1993). SAM is evoked by a stimulus consisting of two images presented alternatingly with a short intermediate blank phase, each showing two illuminated points located at opposite corners of an imaginary rectangle (figure 3, top panel). It conveys the impression of a pair of points oscillating *either* horizontally *or* vertically (figure 3, centre panel). Under certain circumstances the observer might also see a rotation (figure 3, bottom panel).

In analogy with ambivalent figures one finds that the interpretation of the SAM by the visual system at any given time is unique but undergoes spontaneous changes between the alternatives. Furthermore, if the stimulus geometry is asymmetric, i.e. the imaginary rectangle is not a square, subjects seem to favourably perceive motion along its shorter edge; the remaining possibilities are suppressed but still not excluded. When the aspect ratio of the stimulus is continuously varied during presentation, hysteresis occurs. With an initial geometry with one edge being much shorter than the other one the observer will

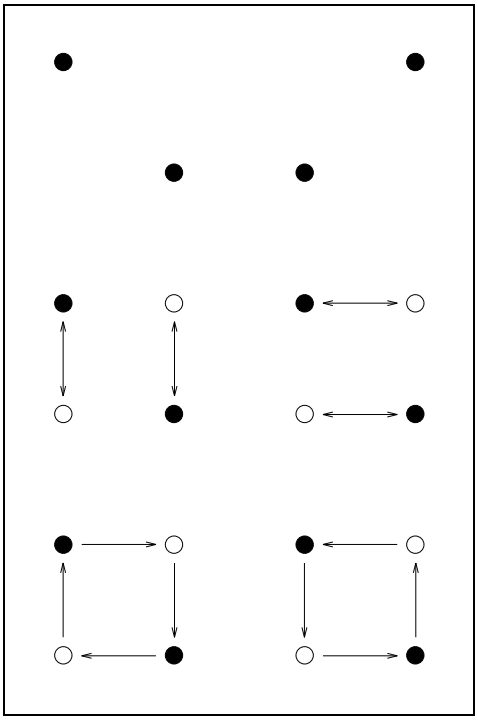

Figure 3. Stroboscopic alternative motion (SAM): the visual interpretation of two alternating images as shown in the top panel can lead to different motion percepts given in the remaining panels.

normally find the points oscillating along this preferred direction. In the course of the stimulus modification to a final configuration with an inverted aspect ratio, however, he will experience a change of his percept such that the points are again moving along the shorter edge. Usually this change of percept occurs at a time when the stimulus is already beyond its symmetric configuration, which is what the term 'hysteresis' refers to.

Since the phenomena described above are similar for the perception of reversible figures and the SAM, two processes that are quite different at first glance, their investigation is a promising way of achieving new insights into fundamental aspects of neural data processing. In fact, many or even most of the data that are to be handled by the neural system are ambiguous. It therefore seems to be a plausible assumption that for their interpretation similar structures have evolved in different areas of the neural system that are concerned with perception.

Many of the more recent analyses of visual ambiguity accept as a premise the ability of the central nervous system to find unambiguous stimulus interpretations and concentrate on mechanisms that might lead to spontaneous or oscillatory changes between different interpretations. The discussed theories comprise stochastic (Borsellino *et al* 1972, Taylor and Aldridge 1974, DeMarco *et al* 1977, Borsellino *et al* 1982), cognitive (Girgus *et al* 1977, Rock and Mitchener 1992, Rock *et al* 1994), and deterministic models (Köhler 1940, Köhler and Wallach 1944, Howard 1961, Orbach *et al* 1963, Spitz 1963, Stadler and Erke 1968, Erke and Gräser 1972, Long and Toppino 1981, Toppino and Long 1987, Ditzinger and Haken 1989, 1990).

A somewhat different approach is to ask the question: 'What are the necessary structures for a neural system to manage the important task of forming a consistent representation of the outside world from the total input of external stimuli?' To answer this question, it might be helpful to develop neural models of the perception of selected examples of ambivalent

stimuli. Such models should be based on functional units that have already been studied and are well understood. Predictions of the models concerning perceptual changes and hysteresis can then be used for comparisons with experimental data.

In what follows we present a neural network model of the SAM perception. An abstract approach to this topic has been published recently by Carmesin and Arndt (1996). In contrast to this work, we develop a microscopic model, which is kept as close as possible to the biological data. In response to the SAM stimulus our network signals either a horizontal or a vertical motion, dependent on the stimulus geometry, and it reproduces hysteresis when the stimulus configuration is continuously varied during the presentation period. The essential ingredients of the model are motion detectors with spatio*temporal* receptive fields that are qualitatively similar to those described by Wimbauer *et al* (1994, 1996).

2. The network

2.1. Motion detectors

In their analyses, Wimbauer *et al* (1994, 1996) have demonstrated how motion-sensitive cells selective to both direction and velocity can emerge in the visual cortex from a Hebbian learning rule. In short, they have shown what the spatio*temporal* receptive fields of these cells may look like; see also DeAngelis *et al* (1995) for experimental data. The mode of operation of such a motion detector can be illustrated by a neuron which receives input from a large number of positions on the retina, each via a large amount of parallel connections. Its output is therefore not determined by the illumination of a single point within the visual field but rather by the stimulus distribution over an extended receptive field. Moreover, each stimulus on the retina is multiply transmitted to the neuron with different delays along the parallel connections. Figure 4 is a schematic sketch of a cell connected four times to each of three positions on the retina.

Since the number of synapses is very large, their spatial distribution combined with

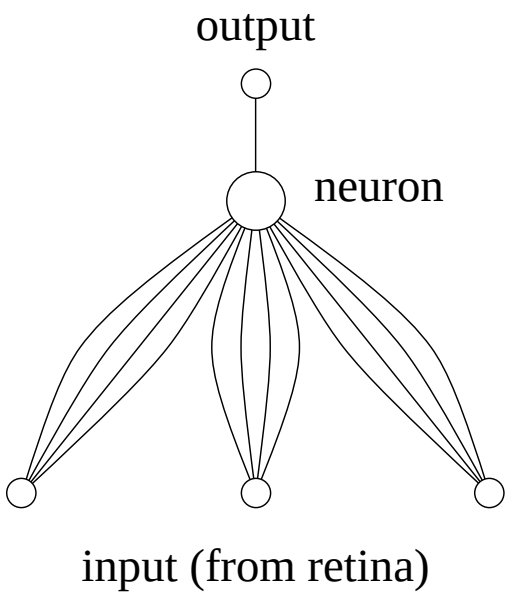

Figure 4. Schematic representation of a neuron which could be tuned to work as a motion detector. Each stimulus is transmitted from the input layer to the neuron along four parallel connections with different delays.

the distribution of delay times is usually approximated by a continuous function $\xi(\boldsymbol{x}, t)$, the spatiotemporal receptive field. The value of $\xi(\boldsymbol{x}, t)$ is to be interpreted as the synaptic weight of a stimulus which is located at a position $\boldsymbol{x}$ within the receptive field and reaches the detector after a time t has elapsed.

The membrane potential of a cell at a given time t is the weighted sum of all signals arriving at the soma at that time. It can be written in the form of a convolution

$$h(\boldsymbol{x}, t) = \int_{-\infty}^{t} \mathrm{d}t' \iint \mathrm{d}^2x'\, \xi\left(\boldsymbol{x}' - \boldsymbol{x}, t - t'\right) s\left(\boldsymbol{x}', t'\right) \tag{1}$$

where $\boldsymbol{x}$ and $s(\boldsymbol{x}, t)$ denote the position of the receptive field on the retina and the time-dependent stimulus distribution, respectively.

The neural model presented here is based on rate-coding neurons with receptive fields which are qualitatively similar to those proposed by Wimbauer *et al* (1996), but are slightly idealized. They are composed of a spatiotemporal part $\xi_1(\boldsymbol{x}, t, \boldsymbol{v})$ multiplied by a purely spatial part $\xi_2(\boldsymbol{x}, \boldsymbol{v})$

$$\xi(\boldsymbol{x}, t, \boldsymbol{v}) := \xi_1(\boldsymbol{x}, t, \boldsymbol{v})\ \xi_2(\boldsymbol{x}, \boldsymbol{v}) .$$

In what follows we let $\boldsymbol{x} := (x, y)$. In our model ξ_1^{x+} for a motion detector tuned to a stimulus velocity v in positive x-direction (indicated by the upper index '$x+$') is then given by

$$\xi_1^{x+}(x, t, v) := \begin{cases} -\xi_0 \dfrac{v}{2\sigma} & \text{if } -2\sigma < v(t - t_0) + x \leqslant -\sigma \\ & \text{or } \sigma < v(t - t_0) + x \leqslant 2\sigma \\ \xi_0 \dfrac{v}{2\sigma} & \text{if } -\sigma < v(t - t_0) + x \leqslant \sigma \\ 0 & \text{otherwise} \end{cases} \tag{2}$$

and ξ_2^{x+} reads

$$\xi_2^{x+}(x, y, v) := \begin{cases} \exp\left(-\dfrac{x^2}{\sigma_\parallel^2} - \dfrac{y^2}{\sigma_\perp^2}\right) & \text{if } -v\, t_{\mathrm{cut}} < x < 0 \\ 0 & \text{otherwise.} \end{cases} \tag{3}$$

Three main ideas have entered the definition of ξ_2. First, there must be some kind of cut-off at some upper bound of x since otherwise the neuron would need connections with negative delay times. For this upper bound we have chosen $x = 0$. Second, assuming that there is not only a minimal but also a maximal signal delay time we have introduced another cut-off at a lower bound $x = -v\, t_{\mathrm{cut}}$. Third, we assume the receptive field of a motion sensitive cell to become gradually weak in the outer regions. To be explicit, we use a two-dimensional Gaussian profile, although our model does not rely on this specific form. Figure 5 illustrates the ansatz

$$\xi^{x+}(x, y, t, v) = \xi_1^{x+}(x, t, v)\ \xi_2^{x+}(x, y, v) \tag{4}$$

for two different values of the velocity v with $t_0 = 30$ ms and $t_{\mathrm{cut}} = 240$ ms.

Using equation (1) one can now derive the membrane potential of a motion detector for any given stimulus distribution. This membrane potential, however, is not the output the neuron provides for further processing. Whereas in biological neural systems information is transmitted in the form of well-separated action potentials called 'spikes', our model uses a rate coding, i.e. the neural output A is a continuous quantity proportional to an

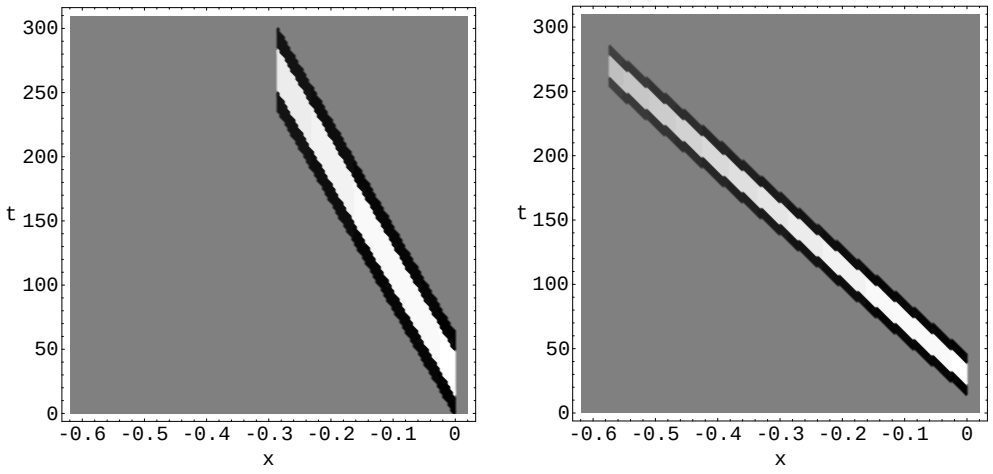

Figure 5. Grey-level plots of the spatiotemporal receptive fields $\xi^{x+}(x, y, t, v)$ of two model neurons sensitive to motion along the positive x-direction at different velocities v and for $y = 0$ (after Wimbauer *et al* 1996). A light or dark shading indicates a positive or a negative coupling ξ^{x+}, respectively, whereas the grey level filling most of the plots means $\xi^{x+} = 0$. The delay time t is given in milliseconds along the vertical axis, the horizontal axis specifies the x-component of the retinal stimulus position in arbitrary units. In our network model this spatial extension of the receptive fields has to be chosen sufficiently large, so that at least some of the neurons can 'see' neighbouring points of the SAM stimulus. The parameters t_0 and t_{cut} have been set to 30 ms and 240 ms, respectively. While the delay time goes up to about 300 ms for both neurons, the receptive field of the motion detector tuned to a higher velocity (right panel) spans a larger distance on the retina. However, at larger distances its amplitude quickly decreases according to a Gaussian, cf equation (3).

effective firing rate. Information which may be encoded in the *exact* temporal sequence of a biological spike train is neglected. As a gain function, we use a nonlinear sigmoidal transfer function

$$A(h) := \tfrac{1}{2}\{1 + \tanh[\beta(h - \theta)]\} \tag{5}$$

with a noise parameter β and a threshold θ to calculate the effective firing rate A of a cell from its membrane potential h.

To demonstrate that the motion detectors introduced so far are not only sensitive to a continuous stimulus motion across their receptive field but also to the apparent motion inherent in the SAM, we have analysed their behaviour in the presence of a 'jumping' point-like stimulus. The left panel of figure 6 shows a grey-level plot of the time-dependent membrane potential of a motion detector for positive x-direction evoked by a stimulus consisting of an illuminated point at a position $\boldsymbol{x} = (-0.22, 0)$ that vanishes at the time $t = 0$ and is replaced at $t = 50$ ms by another illuminated point at the position $\boldsymbol{x} = (-0.02, 0)$. For $t < 0$ as well as for $t > 50$ ms the stimulus is constant, i.e. it is switched on at $t \to -\infty$ and turned off at $t \to +\infty$. As before, we have set $t_0 = 30$ ms and $t_{\text{cut}} = 240$ ms. The parameter v is the velocity of the motion to which the neuron is tuned. Using expression (5) with appropriate values of β and θ one can convert the membrane potential to the firing rate A as plotted in the right panel of figure 6 for $\beta = 30$ and $\theta = 0.65$.

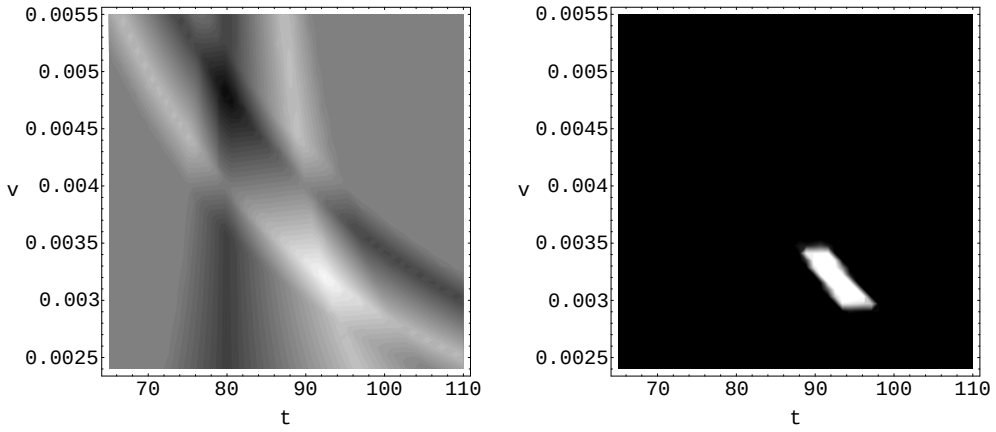

Figure 6. The left panel shows a grey-level plot of the time-dependent membrane potential h of a motion detector for positive x-direction evoked by a stimulus consisting of an illuminated point at a position $\boldsymbol{x} = (-0.22, 0)$ that vanishes at the time $t = 0$ and is replaced at $t = 50$ ms by another illuminated point at the position $\boldsymbol{x} = (-0.02, 0)$. As before, we have set $t_0 = 30$ ms and $t_{\text{cut}} = 240$ ms. The parameter v is the velocity of the motion to which the neuron is tuned. Using expression (5) with $\beta = 30$ and $\theta = 0.65$ the membrane potential can be converted to the firing rate $A(h)$ plotted in the right panel.

2.2. Wiring

Physiological studies have shown that at least the primary visual cortex is organized as a neural map of the retina, i.e. adjacent neurons in the cortex receive their input from adjacent receptive fields on the retina. For this reason one can, as we shall do throughout what follows, identify the 'position' of a neuron with the position of its receptive field on the retina if the relevant region of the cortex is small enough.

The network we have developed is designed to model a small, quadratic patch of the visual cortex. The modelled area is divided into 10×10 fields, each containing 320 neurons, namely 4×80 motion sensitive cells tuned to different velocities v and dedicated to the positive x-, negative x-, positive y-, and negative y-direction. The sizes of their receptive fields parallel and orthogonal to the direction of preferred motion are defined by equation (3) as $\sigma_{\parallel} v$ and $\sigma_{\perp} v$, respectively, where $\sigma_{\parallel}$ and $\sigma_{\perp}$ are model parameters. To ensure that the apparent motion of the SAM can be resolved, they have to be chosen sufficiently large such that a few of the motion detectors can 'see' neighbouring corners of the rectangular stimulus. As a consequence, adjacent receptive fields normally show a very large overlap.

Up to now, we only have a set of motion detectors working independently of one another. Due to the lack of unambiguous experimental results concerning their mutual interactions one has to rely on plausible assumptions. We have decided to introduce a reciprocal inhibition of *orthogonal* directions, i.e. cells sensitive to horizontal and vertical motion inhibit each other (through interneurons), whereas neurons sensitive to motion along parallel or antiparallel directions are left unconnected. This is similar to the mexican-hat-like distribution of weights, which Somers *et al* (1995) used in their model of orientation selectivity in the visual cortex of cats. In addition, we assume the inhibitory contribution that one cell receives at a time t from the activity of another cell at an earlier time t' to depend on their relative distance and to decay exponentially with elapsed time $(t - t')$.

With $h(\boldsymbol{x}', \boldsymbol{v}', t')$ denoting the membrane potential of a neuron located at position $\boldsymbol{x}'$

and tuned to velocity $\boldsymbol{v}'$ the *inhibitory* input $q(\boldsymbol{x}, \boldsymbol{x}', \boldsymbol{v}', t)$ this neuron induces at time t to a cell at position $\boldsymbol{x}$ with $\boldsymbol{v} \perp \boldsymbol{v}'$ can therefore be written in the form

$$q\left(\boldsymbol{x}, \boldsymbol{x}', \boldsymbol{v}', t\right) = \int_{-\infty}^{t} \mathrm{d}t'\, \mu\left(\left|\boldsymbol{x}' - \boldsymbol{x}\right|\right) \exp\left(-\frac{t-t'}{\tau}\right) A\Big[h\left(\boldsymbol{x}', \boldsymbol{v}', t'\right)\Big] \quad (6)$$

where τ is the decay time and $\mu(|\boldsymbol{x}' - \boldsymbol{x}|)$ the weight of inhibition as a function of distance. The membrane potential of any neuron is given by the stimulus input according to equations (1), (2) and (3) minus the sum of inhibitory contributions from all the detectors dedicated to orthogonal directions. In the present context, direct excitatory connections can, and have been neglected. As before, let us use upper indices to indicate the direction of motion to which a cell is sensitive. Then we have

$$h^{x\pm,y\pm}(\boldsymbol{x}, v, t) = \int_{-\infty}^{t} \mathrm{d}t' \iint \mathrm{d}^2x'\, s\left(\boldsymbol{x}', t'\right) \xi^{x\pm,y\pm}\left(\boldsymbol{x}' - \boldsymbol{x}, v, t - t'\right) - \sum_{\boldsymbol{x}', v'} q^{y+,x+}\left(\boldsymbol{x}, \boldsymbol{x}', v', t\right) - \sum_{\boldsymbol{x}', v'} q^{y-,x-}\left(\boldsymbol{x}, \boldsymbol{x}', v', t\right) \quad (7)$$

which is a system of integral equations with one equation per neuron and each neuron characterized by its position $\boldsymbol{x}$, velocity v, and direction $x\pm$, $y\pm$.

To fix $\mu(\boldsymbol{x})$ we assumed that in biological systems the spatial variation in the strength of inhibitory connections is basically determined by the spatial distribution of a neuron's synapses. This distribution might well be the result of a process similar to random walk which takes place when the neuron builds up its dendrites. Thus, a reasonable choice for μ is a Gaussian

$$\mu\,(x) := \mu_0 \exp\left(-\frac{x^2}{\sigma_{\mathrm{inh}}^2}\right) \quad (8)$$

if the width σ_{inh} is chosen appropriately. Since we model only a small region of the visual cortex which is almost fully covered by the SAM stimulus, we apply values of σ_{inh} larger than the size of the network. In this way we ensure that a sufficient interaction is established between cells excited by different parts of the stimulus.

3. Simulation

To investigate the properties of the network described above, we used the stimulus of the SAM but with an aspect ratio varying periodically. Each of the two images was presented for a period corresponding to 200 ms in real time and an intermediate blank phase corresponding to 50 ms was inserted before switching to the next image. The length of the horizontal edge of the stimulus which is relatively short at the beginning (figure 7, left panel) increases gradually, while the vertical distance decreases simultaneously. Once the stimulus takes its second extreme configuration with a short vertical edge (figure 7, right panel) the process reverses and starts anew when the initial state is reached again.

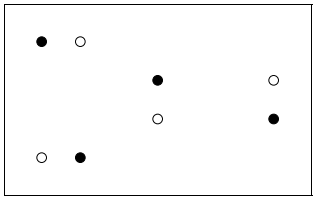

Figure 7. The two extreme configurations of the stimulus of the stroboscopic alternative motion (SAM) presented to the model network.

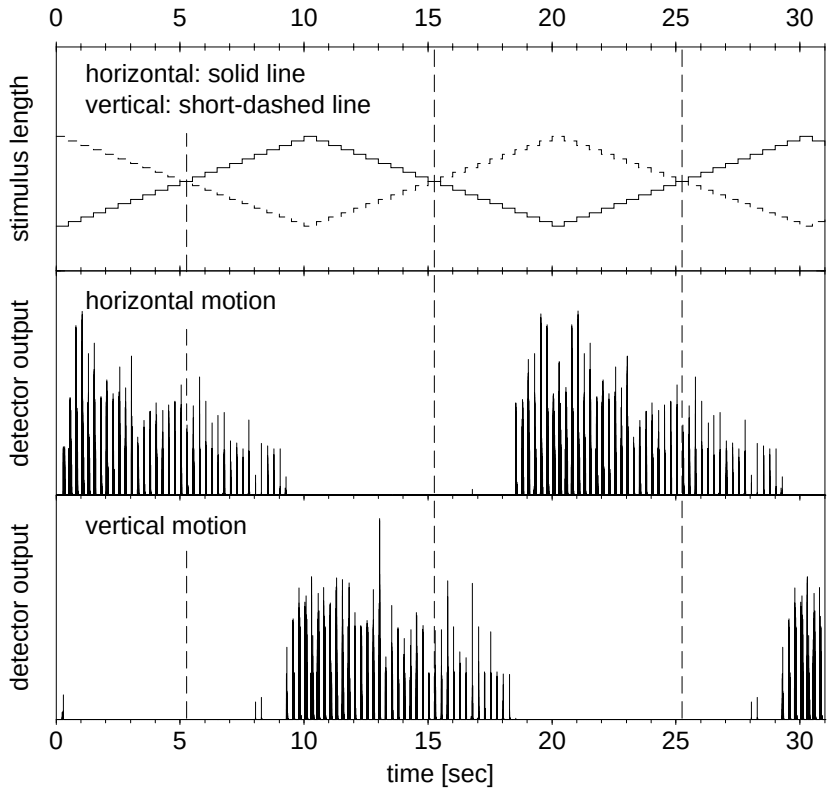

Figure 8. Upper panel: lengths of the horizontal and vertical edges of the SAM stimulus as a function of time and in arbitrary units. Centre and lower panels: mean activity of all detectors of horizontal and vertical motion, respectively. It can be seen that either detectors of horizontal or detectors of vertical motion show a high activity and that a high activity of one network component causes at the same time a suppression of the other component. If the stimulus configuration is highly asymmetric, the detected apparent motion is oriented along the shorter edge of the stimulus. Transitions between the two states show *hysteresis*, i.e. they occur when the stimulus is significantly beyond its symmetric configuration (which is indicated by the dashed vertical lines).

The network response is illustrated in figure 8. The upper panel displays the lengths of the horizontal and vertical edges of the stimulus as a function of time and in arbitrary units. The middle and the lower panel show the mean activity of all detectors of horizontal and vertical motion, respectively. The results are in accordance with the experimental findings presented in section 1.

- Either detectors of horizontal or detectors of vertical motion show a high activity. A high activity of one network component causes a simultaneous suppression of the other component. The stimulus interpretation achieved in this way is unambiguous except for short time intervals, during which a transition between the two states occurs.
- If the stimulus configuration is highly asymmetric, the detected apparent motion is oriented along the shorter edge of the stimulus.
- Transitions between the two states show *hysteresis*, i.e. they occur when the stimulus is significantly beyond its symmetric configuration (which is indicated by the dashed vertical lines in figure 8).

Our neural model does not reproduce the spontaneous changes of percept that have been found in psychological studies. Corresponding to the different theories mentioned in section 1 such changes could be implemented by introducing feedback from higher cortical areas or by adding neural saturation or stochastic processes. However, we decided not to incorporate either of them because at this stage of work any choice would be arbitrary and therefore not give further insight into neural processing in biological systems.

4. Main results of the analytical treatment

The properties of the model network developed in section 2 can in part be understood analytically. In what follows, we are going to present the ansatz of our calculations and their main results, while the reader is referred to the appendix for details.

We start by noting that expression (6) can be written as

$$q\left(\boldsymbol{x}, \boldsymbol{x}', \boldsymbol{v}', t\right) = \int_{-\infty}^{+\infty} \mathrm{d}t'\, \mu\left(\left|\boldsymbol{x}' - \boldsymbol{x}\right|\right) \exp\left(-\frac{t-t'}{\tau}\right) \theta\left(t-t'\right)\, A\Big[h\left(\boldsymbol{x}', \boldsymbol{v}', t'\right)\Big]$$

where $\theta(t)$ denotes the Heaviside step function and $\exp[-(t-t')/\tau]\,\theta(t-t')$ is the Green function of the linear differential operator

$$\widehat{\mathrm{D}} := \frac{1}{\tau} + \frac{\mathrm{d}}{\mathrm{d}t}.$$

We then find that by applying $\widehat{\mathrm{D}}$ the system of integral equations (7) is transformed into the system of differential equations

$$\begin{aligned}\widehat{\mathrm{D}}\, h^{x\pm,y\pm}\left(\boldsymbol{x}, v, t\right) = \widehat{\mathrm{D}}\, S^{x\pm,y\pm}\left(\boldsymbol{x}, v, t\right) - \sum_{\boldsymbol{x}', v'} \mu\left(\left|\boldsymbol{x}' - \boldsymbol{x}\right|\right) \\ \times\left\{A\Big[h^{y+,x+}\left(\boldsymbol{x}', v', t\right)\Big] + A\Big[h^{y-,x-}\left(\boldsymbol{x}', v', t\right)\Big]\right\} \qquad (9)\end{aligned}$$

where we have introduced the abbreviation

$$S^{x\pm,y\pm}\left(\boldsymbol{x}, v, t\right) := \int_{-\infty}^{t} \mathrm{d}t' \iint \mathrm{d}^2x'\; s\left(\boldsymbol{x}', t'\right) \xi^{x\pm,y\pm}\left(\boldsymbol{x}' - \boldsymbol{x}, v, t - t'\right).$$

The fact that the time evolution of the network activity can be described by a set of differential equations reveals that the network dynamics do not have a 'memory'. Rather, at any given time the dynamics are completely determined by the momentary network state, together with the stimulus S and its first derivative.

The weight of inhibition $\mu(x)$ has been defined in (8) as a Gaussian and we have mentioned that we use large values of the width σ_{inh}. Let us therefore approximate $\mu(x)$ by a constant $\overline{\mu}$. We restrict the subsequent analysis to the case of a stimulus for which $S^{x\pm,y\pm}(\boldsymbol{x}, v, t) =: S(t)$ is equal for all motion detectors. Then equation (9) yields

$$\widehat{\mathrm{D}}\, h^{x\pm,y\pm}\left(\boldsymbol{x}, v, t\right) = \widehat{\mathrm{D}} S\left(t\right) - \overline{\mu} \sum_{\boldsymbol{x}', v'} \left\{A\Big[h^{y+,x+}\left(\boldsymbol{x}', v', t\right)\Big] + A\Big[h^{y-,x-}\left(\boldsymbol{x}', v', t\right)\Big]\right\}.$$

It is easy to see that the right-hand side of this expression is independent of $\boldsymbol{x}$ and v and thus is identical for all detectors of horizontal or vertical motion, respectively. The same is, of course, true for the original integral equation (7). As a consequence the membrane potential is equal for all cells dedicated to horizontal or vertical motion, respectively. This means we can drop the variables $\boldsymbol{x}$ and v as well as the signs '+' and '−' in the upper

indices and end up with only two equations

$$\frac{\mathrm{d}h^x(t)}{\mathrm{d}t} = \widehat{\mathrm{D}}S(t) - \nu A\left[h^y(t)\right] - \frac{h^x(t)}{\tau} \tag{10}$$

$$\frac{\mathrm{d}h^y(t)}{\mathrm{d}t} = \widehat{\mathrm{D}}S(t) - \nu A\left[h^x(t)\right] - \frac{h^y(t)}{\tau} \tag{11}$$

where the coupling factor ν arises from multiplying $\overline{\mu}$ by the number of detectors tuned to motion in the x-direction or the number of detectors tuned to motion in the y-direction. Since these two numbers are equal in our model, the same value ν appears in both equations. The quantity h^x is coupled to h^y through $A(h^y)$ and, conversely h^y is influenced by $A(h^x)$, i.e. detectors of horizontal and vertical motion inhibit one another.

By reducing (9) to two differential equations in the two quantities h^x and h^y we have shown that in the case of a constant input $\widehat{\mathrm{D}}S$ and a homogeneous inhibition μ our network is equivalent to a model of two formal graded-response neurons with membrane potential h^x and h^y which both receive the same external input S and inhibit each other via synapses of weight ν (cf figure 9). Equations (10) and (11) can further be simplified by introducing the abbreviations

$$x := \beta\left(h^x - \theta\right)$$

$$y := \beta\left(h^y - \theta\right)$$

$$p := \beta\left(\tau\,\widehat{\mathrm{D}}S - \theta\right)$$

$$\varepsilon := \beta\tau\nu$$

which leads to

$$\tau\frac{\mathrm{d}x}{\mathrm{d}t} = p - x - \frac{\varepsilon}{2}(1 + \tanh y) \tag{12}$$

$$\tau\frac{\mathrm{d}y}{\mathrm{d}t} = p - y - \frac{\varepsilon}{2}(1 + \tanh x)\,. \tag{13}$$

For *constant* p, this system of differential equations is formally identical to a special case of the continuous Hopfield model for two neurons (Hopfield 1984). Since p is determined by the external stimulus $\widehat{\mathrm{D}}S$ it will henceforth be termed 'network input'. The mutual

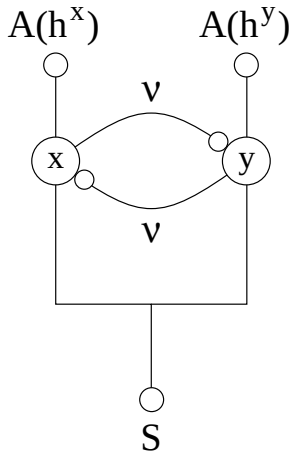

Figure 9. Model of two neurons which both receive the same external input S and inhibit each other via synapses of weight ν.

inhibition which is present in the network is contained in ε, the bifurcation parameter to be. A detailed analysis of equations (12) and (13), carried out in the appendix, yields the following results for any fixed value of p:

- As long as the inhibition, i.e. ε is weak enough, there is exactly *one* fixed point $x(t) \equiv x_0$, $y(t) \equiv y_0 = x_0$. This fixed point is stable and is implicitly given by

$$x_0 = p - \tfrac{1}{2}\varepsilon\,(1 + \tanh x_0)\,.$$

- When ε reaches some critical value $\varepsilon_{\mathrm{cr}}$ a supercritical pitchfork bifurcation occurs, i.e. two additional fixed points $x(t) \equiv x_1$, $y(t) \equiv y_1$ and $x(t) \equiv x_2$, $y(t) \equiv y_2$ emerge with $x_1 < x_0 < x_2$ and $y_1 = x_2$ as well as $y_2 = x_1$. In this regime the new fixed points are stable, while the original one has become unstable. The critical $\varepsilon = \varepsilon_{\mathrm{cr}}$ can be found by solving the equations

$$\varepsilon_{\mathrm{cr}} = \frac{2\left(p - x_0^{\mathrm{cr}}\right)^2}{2\left(p - x_0^{\mathrm{cr}}\right) - 1} \qquad \tanh x_0^{\mathrm{cr}} = 1 - \frac{1}{p - x_0^{\mathrm{cr}}}.$$

- With increasing p the value of $\varepsilon_{\mathrm{cr}}$ decreases as long as $p < 1$ and increases if $p > 1$. The minimum value at $p = 1$ is $\varepsilon_{\mathrm{cr}} = 2$. Figure 10 shows two plots of $\varepsilon_{\mathrm{cr}}$ as a function of p.

Because equations (12) and (13) are directly related to the continuous Hopfield model its Liapunov function (Hopfield 1984) is directly applicable. We therefore know that for constant network input p the system will always converge to one of its fixed points.

If no stimulus is presented to our network or the stimulus presented does not change in time, the external input S of the motion detectors drops to zero, which is below the threshold θ. Hence $p = \beta(S - \theta)$ is negative and $\varepsilon_{\mathrm{cr}}$ decreases with increasing p. We set the inhibitory weight μ such that $2 < \varepsilon < \varepsilon_{\mathrm{cr}}$. Consequently, if p is raised, then the system will eventually enter the critical region because $\varepsilon_{\mathrm{cr}}$ drops below ε; see figure 10. When this happens the system will start drifting to one of the new fixed points, i.e. the detectors of horizontal motion and those of vertical motion will approach different levels of activity. Of course, for the real SAM stimulus the model of two-neurons treated above does not correctly describe the network response, since in this case the assumptions of an equal input to all neurons and a spatially constant inhibition are not valid. However, if we are willing to accept the predictions of this simple model as a rough approximation to the real behaviour, we are able to achieve a qualitative understanding of how hysteresis can emerge.

Suppose the first frame (first pair of bright spots) of the symmetric version of the SAM stimulus has been set and for some reason the neurons dedicated to horizontal motion are at a higher level of activity than those dedicated to vertical motion. The network input p is relatively low so that $\varepsilon < \varepsilon_{\mathrm{cr}}$ and the membrane potential of all motion detectors approaches the same value. When the stimulus switches to the second frame (second pair of bright spots) they receive an external input (cf figure 6), which is equal for both categories of detectors because the stimulus is symmetric. Due to this external input the system is shifted into the critical regime and the membrane potentials begin to drift apart towards values corresponding to one of the system's new fixed points. Since initially the detectors of horizontal motion are at a higher level of activity their membrane potential approaches the higher value and thereby inhibits the detectors of vertical motion, whose membrane potential approaches the lower level.

In this way, the network continues to signal a horizontal motion for the SAM until the asymmetry of the neural activations is overcome by a sufficient asymmetry of the network

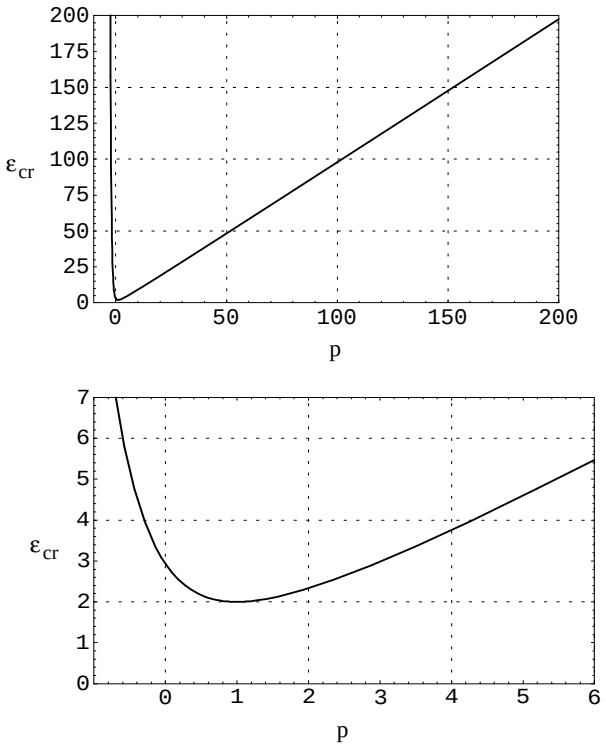

Figure 10. Critical value ε_{cr} of the inhibitory weight ε as a function of the network input p. For $\varepsilon \leqslant \varepsilon_{cr}$ there is only one fixed point of the system of differential equations (10) and (11), for $\varepsilon > \varepsilon_{cr}$ there are three fixed points, two of which are stable. The lower panel is an enlargement of part of the upper one.

input. Such an asymmetry can be inferred by modifying the geometry of the SAM stimulus. Our motion detectors are organized in such a way that they prefer to 'see' an apparent motion along the shorter edge, i.e. the corresponding cells receive a stronger external input, which is due to the definition (3) of the spatial part of the receptive fields. Therefore, if the vertical edge of the stimulus becomes sufficiently short compared with the horizontal edge, the detectors of vertical motion will generate a sufficiently strong output to force the network into a state where neurons dedicated to vertical motion are at a higher level of activity. At this point an equivalent line of arguments makes clear that the network will now indicate vertical motion until the stimulus geometry has again changed to a configuration of a very short horizontal edge. This effect is exactly what we refer to as 'hysteresis'.

5. Conclusions

In the investigation presented here we have developed a microscopic neural model of the stroboscopic alternative motion (SAM). It is based on rate coding and motion-sensitive cells with spatiotemporal receptive fields qualitatively similar to those proposed by Wimbauer *et al* (1994, 1996), which emerge from a Hebbian learning rule. As to the interactions between these motion detectors one is dependent on reasonable assumptions because of the lack of unambiguous experimental data. We have decided to introduce a reciprocal inhibition between cells tuned to orthogonal directions. This seems to be biologically plausible and is analogous to the mexican-hat-like distribution of weights presented by Somers *et al* (1995) in their model of orientation selectivity. Note that we do not use any kind of fast-learning synapses.

Despite its simplicity, the network reproduces the main psychological results concerning the SAM, namely the unambiguous interpretation of the stimulus, preferred detection of motion along the shorter distance and hysteresis. Our analytical treatment has revealed that these properties are due to the following two essential ingredients of the model:

- The spatio-*temporal* receptive fields of the neurons show two important features. First, they enable the cells to 'see' the apparent motion inherent to the SAM. In particular, they are large enough to bind corresponding points of the stimulus. Second, they induce an input to the neurons which is the larger the closer corresponding points are together.
- The reciprocal inhibition of cells tuned to orthogonal directions is below a critical strength if no stimulus is present, whereas the network becomes over-critical when the neurons are sufficiently stimulated. In the former case the detectors of horizontal and those of vertical motion approach the same level of activity. The latter case is characterized by the fact that the two classes of detectors drift towards different levels of activity. One of the groups will exhibit a relatively high firing rate, thereby suppressing neurons of the other class to a lower level of activity.

The above requirements are not very restrictive, i.e. the operation of the network is not limited to the special parametrizations we have chosen for our simulations. Rather, they can be regarded as realizations of quite general and plausible ideas, which, we hope, can be verified experimentally in the near future. Replacing the pools of motion detectors by pools of neurons signalling the overlap between the external stimulus and some given patterns we could apply our model to the perception of ambiguous figures. These facts put a strong emphasis on the biological relevance of the model.

The network we have analysed in this paper consisted of neurons sensitive to horizontal or vertical motion only and the strength of inhibition was approximately constant in space. Future studies can drop these simplification and investigate larger networks which are presented more complicated stroboscopic stimuli. One can think of a whole variety of interesting configurations of stimuli allowing for a detailed comparison between the computational model and psychological experiments.

Appendix. Analytical treatment

In this appendix we present the details of the calculations leading to the results of section 4. There it was demonstrated that the system of integral equations (7) can be transformed into the system of differential equations (9). Furthermore, in the case of a spatially constant inhibition $\overline{\mu}$ and a stimulus S that is equal for all motion detectors, the description of our network reduces to a model of two neurons with membrane potentials h^x and h^y governed by (10) and (11). Subsequently we derive the fixed-point equations for this effective two-neuron model and use bifurcation theory to analyse existence and stability of fixed points in dependence on the mutual inhibition and the network input.

A.1. Fixed-point equations

In section 4 we have already introduced new variables

$$x := \beta\left(h^x - \theta\right) \qquad y := \beta\left(h^y - \theta\right)$$

$$p := \beta\left(\tau\,\widehat{\mathrm{D}}S - \theta\right) \qquad \varepsilon := \beta\tau\nu$$

and obtained

$$\tau \frac{\mathrm{d}x}{\mathrm{d}t} = p - x - \frac{\varepsilon}{2}(1 + \tanh y) \tag{A1}$$

$$\tau \frac{\mathrm{d}y}{\mathrm{d}t} = p - y - \frac{\varepsilon}{2}(1 + \tanh x) \tag{A2}$$

which arise from equations (10) and (11). In what follows, we will always assume $\varepsilon > 0$, i.e. we restrict the analysis to a system of neurons with *inhibitory* interactions.

To find the fixed points $(x_0; y_0)$ of these differential equations we set $\mathrm{d}x/\mathrm{d}t = 0$ and $\mathrm{d}y/\mathrm{d}t = 0$ and obtain the fixed-point equations

$$x_0 = p - \tfrac{1}{2}\varepsilon (1 + \tanh y_0) \tag{A3}$$

$$y_0 = p - \tfrac{1}{2}\varepsilon (1 + \tanh x_0)\,. \tag{A4}$$

From symmetry it is obvious that for a given fixed point (x_0, y_0) one can find a second one by interchanging x_0 and y_0, which is different from the first one if $x_0 \neq y_0$. Moreover, it is clear that the condition (A3) and (A4) imply $\mathrm{d}p/\mathrm{d}t = 0$.

A.2. Linear stability analysis

Suppose now that we have found a fixed point (x_0, y_0). We linearize (A1) and (A2) in the neighbourhood of (x_0, y_0) and find

$$\tau \frac{\mathrm{d}}{\mathrm{d}t}(x - x_0) = -(x - x_0) - \frac{\varepsilon}{2}\operatorname{sech}^2(y_0)(y - y_0) \tag{A5}$$

$$\tau \frac{\mathrm{d}}{\mathrm{d}t}(y - y_0) = -(y - y_0) - \frac{\varepsilon}{2}\operatorname{sech}^2(x_0)(x - x_0)\,. \tag{A6}$$

Using vector notation with

$$\boldsymbol{x} := \begin{pmatrix} x \\ y \end{pmatrix} \qquad \boldsymbol{x}_0 := \begin{pmatrix} x_0 \\ y_0 \end{pmatrix} \qquad C := -\frac{1}{\tau}\begin{pmatrix} 1 & \frac{1}{2}\varepsilon \operatorname{sech}^2 y_0 \\ \frac{1}{2}\varepsilon \operatorname{sech}^2 x_0 & 1 \end{pmatrix}$$

we can write equations (A5) and (A6) in the simple form

$$\frac{\mathrm{d}}{\mathrm{d}t}(\boldsymbol{x} - \boldsymbol{x}_0) = C(\boldsymbol{x} - \boldsymbol{x}_0)$$

a first-order differential equation which describes the *local* behaviour of our formal system of two neurons in a neighbourhood of a fixed point $\boldsymbol{x}_0 = (x_0, y_0)$.

In order to derive a stability criterion for this fixed point, we have to solve for the eigenvalues λ of the matrix C. They are given by

$$\det(C - \lambda \cdot \mathbb{1}) = \left(-\frac{1}{\tau} - \lambda\right)^2 - \frac{\varepsilon^2}{4\tau^2}\operatorname{sech}^2(x_0)\operatorname{sech}^2(y_0) = 0$$

yielding

$$\lambda_{1,2} = -\frac{1}{\tau} \pm \frac{\varepsilon}{2\tau}\operatorname{sech}(x_0)\operatorname{sech}(y_0)\,. \tag{A7}$$

The corresponding eigenvectors $\boldsymbol{x}_1$ and $\boldsymbol{x}_2$ are easily found from

$$\left(C - \lambda_{1,2}\mathbb{1}\right)\boldsymbol{x}_{1,2} = \mathbf{0}$$

and read

$$\boldsymbol{x}_1 = \begin{pmatrix} \operatorname{sech} y_0 \\ -\operatorname{sech} x_0 \end{pmatrix} \qquad \boldsymbol{x}_2 = \begin{pmatrix} \operatorname{sech} y_0 \\ \operatorname{sech} x_0 \end{pmatrix}.$$

A fixed point is stable if both eigenvalues are negative, because then any small perturbation will decay exponentially. On the other hand, if one or both of the eigenvalues are positive a small perturbation will, as long as the linear approximation is valid, increase exponentially. Since $\varepsilon > 0$ and $\tau > 0$ it is evident that the second term of (A7) as well as $1/\tau$ are always positive so that λ_2 (corresponding to the '$-$' sign) is always negative. For λ_1 to be negative, i.e. the fixed point $\boldsymbol{x}_0$ to be stable, we require that

$$\tfrac{1}{2}\varepsilon \operatorname{sech}(x_0)\operatorname{sech}(y_0) < 1. \tag{A8}$$

A.3. Existence of fixed points

In the preceding section we assumed the existence of a fixed point and the analysis of (A1) and (A2) provided us with a criterion for stability. Here we are going to determine how many fixed points exist. We define

$$f(x_0) := \tanh y_0(x_0) \tag{A9}$$

where y_0 is considered as a function of x_0, given by (A4), and written $y_0 = y_0(x_0)$. The first and the second derivative of f are

$$f'(x_0) = -\tfrac{1}{2}\varepsilon \operatorname{sech}^2(x_0)\operatorname{sech}^2(y_0)$$

$$f''(x_0) = \varepsilon \operatorname{sech}^2(x_0)\tanh(x_0)\operatorname{sech}^2(y_0) - \tfrac{1}{2}\varepsilon \operatorname{sech}^4(x_0)\operatorname{sech}^2(y_0)\tanh(y_0)\,.$$

Taking advantage of (A9), from (A3) we obtain a fixed-point equation for x_0:

$$f(x_0) = -\frac{2}{\varepsilon}\,x_0 + \frac{2p}{\varepsilon} - 1. \tag{A10}$$

Both sides of this equation consist of continuous functions, with $f(x_0)$ being bounded by $+1$ and -1, whereas the right-hand side approaches $\pm\infty$ for $x_0 \to \pm\infty$. Consequently, there is at least one point of intersection between their graphs or, in other words, at least one fixed point (cf figure A1, left panel).

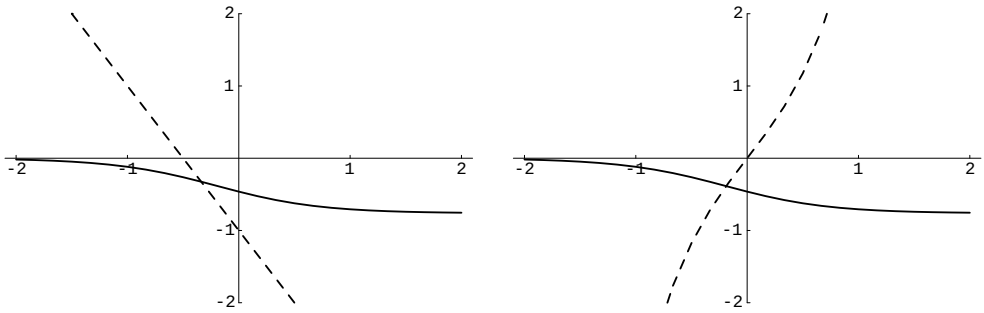

Figure A1. Left panel: the intersection of the graph of $f(x)$ (solid line) with that of $-2x - 1$ (dashed line) represents the solution of (A10) for $\varepsilon = 1$ and $p = 0$. Since there is always *at least* one intersection between the graphs of a bounded function and a straight line with non-zero slope, there is always at least one solution of (A10). Right panel: the solution of (A12) can be visualized as the intersection of the graphs of the bounded function $f(x)$ (solid line) with the unbounded function $\sinh(2x)/\varepsilon$ (dashed line). For this plot, $\varepsilon = 1$ and $p = 0$. As the slopes of the two functions have opposite sign for any p and $\varepsilon > 0$ there is always *exactly* one intersection. In both panels the horizontal axis is the x-axis.

As the solutions of (A10) are the intersections of a monotonically decreasing but bounded function f with a straight line of negative slope, more than one fixed point may exist if $f(x_0)$ turns out to have points of inflexion. Let us therefore look for zeros of $f''(x_0)$, which are solutions of

$$\tfrac{1}{2}\varepsilon \operatorname{sech}^4(x_0)\operatorname{sech}^2(y_0)\tanh(y_0) = \varepsilon \operatorname{sech}^2(x_0)\tanh(x)\operatorname{sech}^2(y_0) \tag{A11}$$

or, after dividing by $(\varepsilon^2/2)\operatorname{sech}^4(x_0)\operatorname{sech}^2(y_0)$ and substituting $f(x_0) = \tanh(y_0)$,

$$f(x_0) = \frac{2}{\varepsilon}\sinh(x_0)\cosh(x_0) = \frac{1}{\varepsilon}\sinh(2x_0)\,. \tag{A12}$$

Differentiating the functions on both sides of this equation, one finds that their slopes have opposite sign. Together with the fact that they both are continuous and that $\sinh(2x_0)$ approaches $\pm\infty$ for $x_0 \to \pm\infty$, it follows that $f''(x_0)$ has exactly one zero (cf figure A1, right panel). On the other hand, since f is continuous and bounded, has a continuous first derivative, and $\lim_{x_0\to-\infty} f(x_0) \neq \lim_{x_0\to+\infty} f(x_0)$, there must be at least one point of inflexion. At any point of inflexion, however, we have $f''(x_0) = 0$, because $f''(x_0)$ is continuous. So, finally, we know $f(x_0)$ to have exactly one point of inflexion, which implies that equation (A10) gives rise to either 1, 2, or 3 fixed points. We are now interested in the number of fixed points in dependence on ε.

For $x_0 = y_0$ the fixed-point equations (A3) and (A4) reduce to

$$x_0 = p - \tfrac{1}{2}\varepsilon\,(1 + \tanh x_0)\,. \tag{A13}$$

Since $y(x) = p - \frac{1}{2}\varepsilon(1 + \tanh x)$ is a monotonically decreasing function, there is exactly one intersection with the straight line $y = x$ yielding exactly one solution of (A13) for *any* value of ε. For very small (positive) values of ε equation (A10) yields only one fixed point, which must therefore correspond to the solution of (A13). Moreover, relation (A8) shows that this fixed point is stable.

As explained above, at most two additional fixed points can arise as ε increases. Since there is exactly one fixed point with $x_0 = y_0$ for any value of ε, namely the solution of (A13), we are bound to find $x_0 \neq y_0$ for any additional fixed point (x_0, y_0). It has been stated before (in section A.1) that, because of the symmetry of the fixed-point equations, from any given fixed point (x_0, y_0) with $x_0 \neq y_0$ a second one can be constructed by interchanging x_0 and y_0. Additional fixed points can therefore only arise as a pair $\{(x_0, y_0), (y_0, x_0)\}$.

Altogether, these considerations lead to the result that our system has exactly one fixed point for sufficiently small values of ε and might undergo a supercritical pitchfork bifurcation once ε reaches a critical value $\varepsilon_{\mathrm{cr}}$. At the bifurcation point the fixed point with $x_0 = y_0$ becomes unstable. Hence we can obtain the critical value $\varepsilon_{\mathrm{cr}}$ from the stability criterion (A8) by requiring

$$\tfrac{1}{2}\varepsilon_{\mathrm{cr}}\operatorname{sech}\left(x_0^{\mathrm{cr}}\right)\operatorname{sech}\left(y_0^{\mathrm{cr}}\right) = \tfrac{1}{2}\varepsilon_{\mathrm{cr}}\operatorname{sech}^2\left(x_0^{\mathrm{cr}}\right) = 1. \tag{A14}$$

Using equations (A13) and (A14) one can easily derive that the bifurcation point is given by

$$\varepsilon_{\mathrm{cr}} = \frac{2\left(p - x_0^{\mathrm{cr}}\right)^2}{2\left(p - x_0^{\mathrm{cr}}\right) - 1} \tag{A15}$$

with

$$\tanh x_0^{\mathrm{cr}} = 1 - \frac{1}{p - x_0^{\mathrm{cr}}} \tag{A16}$$

as stated in section 4.

A.4. Dependence of $\varepsilon_{\rm cr}$ on the network input

The above calculations have revealed the existence of a critical value $\varepsilon_{\rm cr}$ of the inhibitory weight ε at which the system of differential equations (A1) and (A2) changes its properties. Whereas there is exactly one fixed point for $\varepsilon \leqslant \varepsilon_{\rm cr}$ two additional fixed points emerge for larger values of ε. Here we will study the dependence of $\varepsilon_{\rm cr}$ on the network input.

Differentiating equation (A16) with respect to p, we obtain

$$\frac{\mathrm{d}}{\mathrm{d}p}\tanh x_0^{\rm cr} = \frac{1}{\left(p - x_0^{\rm cr}\right)^2}\left(1 - \frac{\mathrm{d}x_0^{\rm cr}}{\mathrm{d}p}\right)$$

yielding

$$\frac{\mathrm{d}x_0^{\rm cr}}{\mathrm{d}p} = \frac{1}{\left(p - x_0^{\rm cr}\right)^2 \operatorname{sech}^2 x_0^{\rm cr} + 1}.$$

Since $(p - x_0^{\rm cr})^2 > 0$ and $\operatorname{sech}^2 x_0^{\rm cr} > 0$ the denominator on the right-hand side exceeds 1 and hence

$$0 < \frac{\mathrm{d}x_0^{\rm cr}}{\mathrm{d}p} < 1. \tag{A17}$$

From equation (A15) we now obtain

$$\frac{\mathrm{d}\varepsilon_{\rm cr}}{\mathrm{d}p} = \left\{1 - \frac{1}{\left[2\left(p - x_0^{\rm cr}\right) - 1\right]^2}\right\}\left(1 - \frac{\mathrm{d}x_0^{\rm cr}}{\mathrm{d}p}\right)$$

and find

$$\frac{\mathrm{d}\varepsilon_{\rm cr}}{\mathrm{d}p}\begin{cases} < 0 & \text{if } p - x_0^{\rm cr} < 1 \\ = 0 & \text{if } p - x_0^{\rm cr} = 1 \\ > 0 & \text{if } p - x_0^{\rm cr} > 1 \end{cases} \tag{A18}$$

because equation (A16) implies $p - x_0^{\rm cr} > 0$ and the inequality (A17) yields $\mathrm{d}(p - x_0^{\rm cr})/\mathrm{d}p = 1 - \mathrm{d}x_0^{\rm cr}/\mathrm{d}p > 0$. As a consequence of (A16) we have $x_0^{\rm cr} = 0$ for $p - x_0^{\rm cr} = 1$, so that equation (A18) is equivalent to

$$\frac{\mathrm{d}\varepsilon_{\rm cr}}{\mathrm{d}p}\begin{cases} < 0 & \text{if } p < 1 \\ = 0 & \text{if } p = 1 \\ > 0 & \text{if } p > 1. \end{cases}$$

At $p = 1$ the critical value of the inhibitory weight takes its minimum $\varepsilon_{\rm cr} = 2$. Figure 10 shows two plots of $\varepsilon_{\rm cr}$ as a function of p.

References

Attneave F 1971 Multistability in perception *Scientific American* **225** 62–71

Borsellino A, Carlini F, Riani M, Tuccio M. T, DeMarco A, Penengo P and Trabucco A 1982 Effects of visual angle on perspective reversal for ambiguous patterns *Perception* **11** 263–73

Borsellino A, DeMarco A, Allazetta A, Rinesi S and Bartolini B 1972 Reversal time distribution in the perception of visual ambiguous stimuli *Kybernetik* **10** 139–44

Botwinick J 1961 Husband and father-in-law: a reversible figure *Am. J. Psychol.* **74** 312–3

Bugelski B R and Alampay D A 1961 The role of the frequency in developing perceptual sets *Can. J. Psychol.* **15** 205–11

Carmesin H and Arndt S 1996 A neural network model for stroboscopic alternative motion *Biol. Cybern.* **75** 239–51

DeAngelis G C, Ohzawa I and Freeman R D 1995 Receptive-field dynamics in the central visual pathways *Trends in Neurosci.* **18** 451–8

DeMarco A, Penengo P, Trabucco A, Borsellino A, Carlini F, Riani M and Tuccio M T 1977 Stochastic models and fluctuations in reversal time of ambiguous figures *Perception* **6** 645–56

Ditzinger T and Haken H 1989 Oscillations in the perception of ambiguous patterns. A model based on synergetics *Biol. Cybern.* **61** 279–87

Ditzinger T and Haken H 1990 The impact of fluctuations on the recognition of ambiguous patterns *Biol. Cybern.* **63** 453–6

Eichler W 1930 Der rhythmische Wechsel in der Auffassung räumlich-zweideutiger geometrischer Figuren *Z. Sinnesphysiol.* **61** 154–93

Epstein W and Rock I 1960 Perceptual set as an artifact of recency *Am. J. Psychol.* **73** 214–28

Erke H and Gräser H 1972 Reversibility of perceived motion: selective adaptation of the human visual system to speed, size and orientation *Vision Res.* **12** 69–87

Girgus J J, Rock I and Egatz R 1977 The effect of knowledge of reversibility on the reversibility of ambiguous figures *Perception Psychophys.* **22** 550–6

Hill W E 1915 My wife and my mother in law *Puck*, 6 November

Hock H S, Kelso J A S and Schöner G 1993 Bistability and hysteresis in the organization of apparent motion patterns *J. Exp. Psychol.* **19** 63–80

Hoeth F 1968 Bevorzugte Richtungen bei stroboskopischen Alternativbewegungen *Psychologische Beiträge* **16** 494–527

Hopfield J J 1984 Neurons with graded response have computational properties like those of two-state neurons *Proc. Natl Acad. Sci. USA* **81** 3088–92

Howard I P 1961 An investigation of an satiation process in the reversible perspective of revolving skeletal shapes *Quart. J. Exp. Psychol.* **13** 19–23

Jastrow J 1900 *Fact and Fable in Psychology* (New York: Houghton Mifflin)

Kawamoto A H and Anderson J A 1985 A neural network model of multistable perception *Acta Psychol.* **59** 35–65

Köhler W 1940 *Dynamics in Psychology* (New York: Liveright)

Köhler W and Wallach H 1944 Figural after-effects: an investigation of visual processes *Proc. Am. Phil. Soc.* **88** 269–357

Kruse P, Stadler M and Wehner T 1986 Direction and frequency specific processing in the perception of long-range apparent movement *Vision Res.* **26** 327–35

Long G M and Toppino T C 1981 Multiple representations of the same reversible figure: Implications for cognitive decisional interpretations *Perception* **10** 231–4

Marbe K 1893 Die Schwankungen der Gesichtsempfindungen *Phil. Stud.* **8** 615–37

Necker L A 1832 Observations on some remarkable phenomena seen in Switzerland; and an optical phenomenon which occurs on viewing of a crystal or geometrical solid *Phil. Mag.* **3** ser. 1 329–43

Orbach J, Ehrlich D and Heath H A 1963 Reversibility of the Necker cube. I. An examination of the concept of 'satiation of orientation' *Percept. Mot. Skills* **17** 439–58

Pöppel E 1982 *Lust und Schmerz. Neuronale Grundlagen menschlichen Verhaltens* (Berlin: Severin and Siedler)

Ramachandran V S 1992 Perception: a biological perspective *Neural Networks for Vision and Image Processing* ed G A Carpenter and S Grossberg (Cambridge, MA: MIT Press) pp 45–91

Ramachandran V S and Anstis S M 1983 Perceptual organisation in moving displays *Nature* **304** 529–31

Ramachandran V S and Anstis S M 1985 Perceptual organization in multistable apparent motion *Perception* **14** 135–43

Rock I, Hall S and Davis J 1994 Why do ambiguous figures reverse? *Acta Psychologica* **87** 33–59

Rock I and Mitchener K 1992 Further evidence of failure of reversal of ambiguous figures by uninformed subjects *Perception* **21** 39–45

Rubin E 1921 *Visuell wahrgenommene Figuren* (Copenhagen: Gyldendalske)

von Schiller P 1933 Stroboskopische Alternativbewegungen *Psychologische Forschung* **17** 179–214

Somers D C, Nelson S B and Sur M 1995 An emergent model of orientation selectivity in cat visual cortical simple cells *J. Neurosci.* **15** 5448–65

Spitz H H 1963 Some experiments with a stationary and revolving three-dimensional skeletal cube, Paper presented at Meeting of the Eastern Psychological Association, New York City, April 1963

Stadler M and Erke H 1968 Über einige periodische Vorgänge in der Figuralwahrnehmung *Vision Res.* **8** 1081–92

Taylor M M and Aldridge K D 1974 Stochastic processes in reversing figure perception *Perception Psychophys.* **16** 9–27

Toppino T C and Long G M 1987 Selective adaptation with reversible figures: don't change that channel *Perception Psychophys.* **42** 37–48

Wallach H and Austin P 1954 Recognition and localization of visual traces *Am. J. Psychol.* **67** 338–40
Wertheimer M 1923 Untersuchungen zur Lehre von der Gestalt: II *Psychologische Forschung* **4** 301–50
Wimbauer S, Gerstner W and van Hemmen J L 1994 Emergence of spatio-temporal receptive fields and its application to motion detection *Biol. Cybern.* **72** 81–92
Wimbauer S, Miller K D and van Hemmen J L 1996 Development of spatiotemporal receptive fields of simple cells *Preprint* TU München